

|              |   |
|--------------|---|
| Title        | Quasifree neutron knockout from $^{54}\text{Ca}$ corroborates arising $N = 34$ neutron magic number   |
| Author(s)    | Chen S., Lee J., Doornenbal P., Obertelli A., Barbieri C., Chazono Yoshiki, Navrátil P., Ogata Kazuyuki, Otsuka Takaharu, Raimondi F., Somà V., Utsuno Yutaka, Yoshida Kazuki, Baba Hidetada, Browne F., Calvet D., Château F., Chiga Nobuyuki, Corsi A., Cortés M. L., Delbart A., Gheller J.-M., Giganon A., Gillibert A., Hilaire S., Isobe Tadaaki, Kahlbow J., Kobayashi Toshio, Kubota Yuki, Lapoux V., Liu H. N., Motobayashi Toru, Murray I., Otsu Hideaki, Panin V., Paul N., Rodriguez W., Sakurai Hiroyoshi, Sasano Masaki, Steppenbeck D., Stuhl D., Sun Y. L., Togano Yasuhiro, Uesaka Tomohiro, Wimmer K., Yoneda Kenichiro, Achouri N., Aktas O., Aumann T., Chung L. X., Flavigny F., Franchoo S., Gašparić I., Gerst R.-B., Gibelin J., Hahn K. I., Kim D., Koiwai Takuma, Kondo Yosuke, Koseoglou P., Lehr C., Linh B. D., Lokotko T., MacCormick M., Moschner K., Nakamura Takashi, Park S. Y., Rossi D., Sahin E., Sohler D., Söderström P.-A., Takeuchi Satoshi, Törnqvist H., Vaquero V., Wagner V., Wang S., Werner V., Xu X., Yamada Hiroki, Yan D., Yang Z., Yasuda Masahiro, Zanetti L. |
| Citation     | Physical Review Letters, 123(14), p.142501_1-142501_7   |
| Text Version | Published Journal Article   |
| URL          | <a href="https://jopss.jaea.go.jp/search/servlet/search?5066827">https://jopss.jaea.go.jp/search/servlet/search?5066827</a>   |
| DOI          | <a href="https://doi.org/10.1103/PhysRevLett.123.142501">https://doi.org/10.1103/PhysRevLett.123.142501</a>   |
| Right        | ©2019 American Physical Society   |

## Quasifree Neutron Knockout from $^{54}\text{Ca}$ Corroborates Arising $N = 34$ Neutron Magic Number

S. Chen<sup>1,2,3,\*</sup>, J. Lee,<sup>1,†</sup> P. Doornenbal,<sup>2</sup> A. Obertelli,<sup>4,2,5</sup> C. Barbieri,<sup>6</sup> Y. Chazono,<sup>7</sup> P. Navrátil,<sup>8</sup> K. Ogata,<sup>7</sup> T. Otsuka,<sup>2,9,10</sup> F. Raimondi,<sup>11</sup> V. Somà,<sup>4</sup> Y. Utsuno,<sup>12,9</sup> K. Yoshida,<sup>12,7</sup> H. Baba,<sup>2</sup> F. Browne,<sup>2</sup> D. Calvet,<sup>4</sup> F. Château,<sup>4</sup> N. Chiga,<sup>2</sup> A. Corsi,<sup>4</sup> M. L. Cortés,<sup>2</sup> A. Delbart,<sup>4</sup> J.-M. Gheller,<sup>4</sup> A. Giganon,<sup>4</sup> A. Gillibert,<sup>4</sup> C. Hilaire,<sup>4</sup> T. Isobe,<sup>2</sup> J. Kahlbow,<sup>5,2</sup> T. Kobayashi,<sup>13</sup> Y. Kubota,<sup>2,14</sup> V. Lapoux,<sup>4</sup> H. N. Liu,<sup>4,15,5</sup> T. Motobayashi,<sup>2</sup> I. Murray,<sup>16,2</sup> H. Otsu,<sup>2</sup> V. Panin,<sup>2</sup> N. Paul,<sup>4</sup> W. Rodriguez,<sup>17,2</sup> H. Sakurai,<sup>2,18</sup> M. Sasano,<sup>2</sup> D. Steppenbeck,<sup>2</sup> L. Stuhl,<sup>14</sup> Y. L. Sun,<sup>4,5</sup> Y. Togano,<sup>19</sup> T. Uesaka,<sup>2</sup> K. Wimmer,<sup>18</sup> K. Yoneda,<sup>2</sup> N. Achouri,<sup>4</sup> O. Aktas,<sup>15</sup> T. Aumann,<sup>5,20</sup> L. X. Chung,<sup>21</sup> F. Flavigny,<sup>16</sup> S. Franchoo,<sup>16</sup> I. Gašparić,<sup>22,2</sup> R.-B. Gerst,<sup>23</sup> J. Gibelin,<sup>24</sup> K. I. Hahn,<sup>25</sup> D. Kim,<sup>25,2</sup> T. Koiwai,<sup>18</sup> Y. Kondo,<sup>26</sup> P. Koseoglou,<sup>5,20</sup> C. Lehr,<sup>5,2</sup> B. D. Linh,<sup>21</sup> T. Lokotko,<sup>1</sup> M. MacCormick,<sup>16</sup> K. Moschner,<sup>23</sup> T. Nakamura,<sup>26</sup> S. Y. Park,<sup>25,2</sup> D. Rossi,<sup>5</sup> E. Sahin,<sup>27</sup> D. Sohler,<sup>28</sup> P.-A. Söderström,<sup>5</sup> S. Takeuchi,<sup>26</sup> H. Törnqvist,<sup>5,20</sup> V. Vaquero,<sup>29</sup> V. Wagner,<sup>5,2</sup> S. Wang,<sup>30</sup> V. Werner,<sup>5</sup> X. Xu,<sup>1</sup> H. Yamada,<sup>26</sup> D. Yan,<sup>30</sup> Z. Yang,<sup>2</sup> M. Yasuda,<sup>26</sup> and L. Zanetti<sup>5,2</sup>

<sup>1</sup>Department of Physics, The University of Hong Kong, Pokfulam, 999077, Hong Kong

<sup>2</sup>RIKEN Nishina Center, Wako, Saitama 351-0198, Japan

<sup>3</sup>School of Physics and State Key Laboratory of Nuclear Physics and Technology, Peking University, Beijing 100871, China

<sup>4</sup>IRFU, CEA, Université Paris-Saclay, 91191 Gif-sur-Yvette, France

<sup>5</sup>Institut für Kernphysik, Technische Universität Darmstadt, 64289 Darmstadt, Germany

<sup>6</sup>Department of Physics, University of Surrey, Guildford GU2 7XH, United Kingdom

<sup>7</sup>Research Center for Nuclear Physics (RCNP), Osaka University, Ibaraki 567-0047, Japan

<sup>8</sup>TRIUMF, 4004 Westbrook Mall, Vancouver, BC, V6T 2A3, Canada

<sup>9</sup>Department of Physics and Center for Nuclear Study, University of Tokyo, Hongo, Bunkyo-ku, Tokyo 113-0033, Japan

<sup>10</sup>Instituut voor Kern- en Stralingsfysica, Katholieke Universiteit Leuven, B-3001 Leuven, Belgium

<sup>11</sup>ESNT, CEA, Université Paris-Saclay, 91191 Gif-sur-Yvette, France

<sup>12</sup>Advanced Science Research Center, Japan Atomic Energy Agency, Tokai, Ibaraki 319-1195, Japan

<sup>13</sup>Department of Physics, Tohoku University, Sendai 980-8578, Japan

<sup>14</sup>Center for Nuclear Study, University of Tokyo, RIKEN campus, Wako, Saitama 351-0198, Japan

<sup>15</sup>Department of Physics, Royal Institute of Technology, SE-10691 Stockholm, Sweden

<sup>16</sup>Institut de Physique Nucléaire, CNRS-IN2P3, Univ. Paris-Sud, Université Paris-Saclay, 91406 Orsay Cedex, France

<sup>17</sup>Universidad Nacional de Colombia, Sede Bogotá, Facultad de Ciencias, Departamento de Física, Bogotá 111321, Colombia

<sup>18</sup>Department of Physics, University of Tokyo, 7-3-1 Hongo, Bunkyo, Tokyo 113-0033, Japan

<sup>19</sup>Department of Physics, Rikkyo University, 3-34-1 Nishi-Ikebukuro, Toshima, Tokyo 172-8501, Japan

<sup>20</sup>GSI Helmholtzzentrum für Schwerionenforschung GmbH, 64291 Darmstadt, Germany

<sup>21</sup>Institute for Nuclear Science and Technology, VINATOM, P.O. Box 5T-160, Nghia Do, Hanoi, Vietnam

<sup>22</sup>Ruđer Bošković Institute, Bijenička cesta 54, 10000 Zagreb, Croatia

<sup>23</sup>Institut für Kernphysik, Universität zu Köln, 50923 Köln, Germany

<sup>24</sup>LPC Caen, ENSICAEN, Université de Caen, CNRS/IN2P3, F-14050 Caen, France

<sup>25</sup>Department of Science Education and Department of Physics, Ewha Womans University, Seoul 03760, Korea

<sup>26</sup>Department of Physics, Tokyo Institute of Technology, 2-12-1 O-Okayama, Meguro, Tokyo 152-8551, Japan

<sup>27</sup>Department of Physics, University of Oslo, N-0316 Oslo, Norway

<sup>28</sup>Institute for Nuclear Research of the Hungarian Academy of Sciences (MTA Atomki), P.O. Box 51, Debrecen H-4001, Hungary

<sup>29</sup>Instituto de Estructura de la Materia, CSIC, 28006 Madrid, Spain

<sup>30</sup>Institute of Modern Physics, Chinese Academy of Sciences, Lanzhou 730000, China



(Received 9 June 2019; published 30 September 2019)

Exclusive cross sections and momentum distributions have been measured for quasifree one-neutron knockout reactions from a  $^{54}\text{Ca}$  beam striking on a liquid hydrogen target at  $\sim 200$  MeV/u. A significantly larger cross section to the  $p_{3/2}$  state compared to the  $f_{5/2}$  state observed in the excitation of  $^{53}\text{Ca}$  provides direct evidence for the nature of the  $N = 34$  shell closure. This finding corroborates the arising of a new shell closure in neutron-rich calcium isotopes. The distorted-wave impulse approximation reaction formalism with shell model calculations using the effective GXPFBs interaction and *ab initio* calculations concur our experimental findings. Obtained transverse and parallel momentum distributions demonstrate the sensitivity of quasifree one-neutron knockout in inverse kinematics on a thick liquid hydrogen target with the reaction vertex reconstructed to final state spin-parity assignments.

DOI: 10.1103/PhysRevLett.123.142501

Nuclear shell structure, as correctly described by Mayer and Jensen 70 years ago with the inclusion of an appropriate spin-orbit force [1,2], embodies the backbone of our understanding of the many-body structure of atomic nuclei. It is characterized by “magic numbers,” which correspond to large energy gaps between single-particle orbitals of protons or neutrons. The magic numbers comprise  $Z$  or  $N$  equal to 2, 8, 20, 28, 50, 82, 126, ..., where  $Z$  and  $N$  denote, respectively, proton and neutron numbers [1,2]. These “canonical” magic numbers are well established for stable nuclei and nuclei located in their vicinity of the nuclear chart. In the past decades, the front line of nuclear structure physics moved gradually to nuclei with large  $N$  vs  $Z$  imbalance, known as exotic nuclei or rare isotopes. As a crucial outcome of these studies, the known set of magic numbers from stable nuclei may not extend their universality to exotic nuclei: Certain magic numbers do not manifest themselves in some nuclei [3–7], while new ones seem to emerge in others [8–12]. Thus, the possible variations of the magic numbers across the nuclear chart are of current intense interest [13,14].

Neutron-rich  $pf$  shell nuclei provide us with an excellent region in the nuclear chart to explore these variations. In fact, a possible new magic number at  $N = 32$  has been investigated abundantly over the past decades: Experimental indications were found for Ar in Ref. [15], for Ca in Refs. [11,16,17], for Ti in Refs. [18–21], and for Cr in Refs. [22,23], by measurements of first  $2^+$  energies [ $E(2_1^+)$ ], reduced transition probabilities to these states [ $B(E2; 0_{gs}^+ \rightarrow 2_1^+)$ ], and mass measurements. More interestingly, by adding only two more neutrons, also a  $N = 34$  subshell gap was suggested by some theories [24,25]. In the framework of tensor-force-driven shell evolution [14,24,26], the formation of the  $N = 34$  subshell gap was associated with the  $\pi f_{7/2}$ - $\nu f_{5/2}$  (proton  $f_{7/2}$ -neutron  $f_{5/2}$ ) nucleon-nucleon attractive interaction [24]. When approaching  $Z = 20$  from “above,” the strength of the attraction between  $\pi f_{7/2}$  and  $\nu f_{5/2}$  becomes weaker due to the decreasing occupation of the  $\pi f_{7/2}$  orbital [27]. Consequently, the  $\nu f_{5/2}$  orbital shifts up in energy and a sizable energy gap emerges between  $\nu p_{1/2}$  and  $\nu f_{5/2}$  at  $Z = 20$  [12,27]. However, such an  $N = 34$  subshell gap was not observed experimentally in Ti [20,28] and Cr [22,23] isotopes. First indications for a sizable  $N = 34$  subshell gap in  $^{54}\text{Ca}$  were presented by the measured large  $E(2_1^+)$  [12] and mass measurements of  $^{55-57}\text{Ca}$  isotopes [29]. This gap seems preserved in the argon isotopes [30].

Magicity is characterized by the closed-shell formation at the magic number. Although the measured  $E(2_1^+)$  and  $S_{2n}$  are consistent with the appearance of a  $N = 34$  magic number, the strength of the shell closure is not well studied. In order to confirm experimentally the  $N = 34$  new magic number, we present a stringent test by probing the ground state wave function of  $^{54}\text{Ca}$  from the quasifree  $^{54}\text{Ca}(p, pn)^{53}\text{Ca}$  neutron knock-out reaction cross sections.

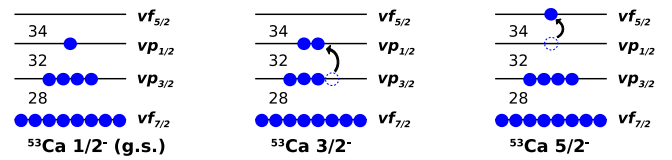


FIG. 1. Illustration of the most representative neutron single-particle configurations for ground and bound excited states of  $^{53}\text{Ca}$ .

In a simple single particle shell model picture (Fig. 1), the  $^{53}\text{Ca}$  ground state has the unpaired neutron occupying the  $\nu p_{1/2}$  orbital and, therefore, assigned to spin parity of  $1/2^-$ . Two excited states have been observed from previous experiments [12,31], tentatively assigned to spin-parities of  $3/2^-$  and  $5/2^-$ , guided mainly by shell model (SM) calculations, thus lacking firm experimental verification on their ordering. Population to each final bound state in  $^{53}\text{Ca}$  can be associated with neutron removal from the specific orbital. In this experiment, partial cross sections feeding to individual  $^{53}\text{Ca}$  final states were measured. In addition, momentum distributions of the  $^{53}\text{Ca}$  residues were investigated, providing the first direct experimental evidence for spin-parity assignments of bound levels in  $^{53}\text{Ca}$ .

The experiment was carried out at the Radioactive Isotope Beam Factory (RIBF), operated by the RIKEN Nishina Center and the Center for Nuclear Study, the University of Tokyo. A  $^{70}\text{Zn}$  primary beam was accelerated to 345 MeV/ $u$  and impinged on a 10-mm-thick  $^9\text{Be}$  production target placed at the entrance of the BigRIPS fragment separator [32]. Fragmentation products were separated using the  $B\rho$ - $\Delta E$ - $B\rho$  method [33]. Beam particles were identified event by event based on the measurements of time-of-flight (TOF), magnetic rigidity ( $B\rho$ ), and energy loss ( $\Delta E$ ) [34]. The primary beam intensity was  $\sim 240$  pA on average, and the rate of  $^{54}\text{Ca}$  in BigRIPS was 7.3 particles/sec. The  $^{54}\text{Ca}$  beam bombarded the 151(1)-mm-thick liquid hydrogen target of the MINOS device [35] with a center-of-target energy of 216 MeV/ $u$ . Reaction residues were identified by the SAMURAI spectrometer following a similar method as for BigRIPS [36].

A 300-mm-long cylindrical time projection chamber (TPC) surrounded the target to measure the trajectory of the recoiled proton. The proton trajectory together with the beam track, determined by drift chambers, was used to reconstruct the reaction vertex in the target [35,36]. For the  $^{54}\text{Ca}(p, pn)^{53}\text{Ca}$  channel, the reconstructed vertex position was obtained with a spatial resolution of 5 mm (FWHM) along the beam axis and the efficiency was obtained to be 70(2)%, by comparing the  $\gamma$ -spectrum photopeak statistics with and without the coincidence of the vertex [37]. To tag on the final states of  $^{53}\text{Ca}$  residues, deexcitation  $\gamma$  rays were measured by the DALI2<sup>+</sup> detector array [38,39], which consisted of 226 NaI(Tl) detectors. Detectors in the array were calibrated individually using  $^{60}\text{Co}$ ,  $^{137}\text{Cs}$ , and  $^{88}\text{Y}$  sources. From the simulation of the GEANT4 framework

[40], a full-energy peak efficiency of 23% was obtained with add back for 2-MeV  $\gamma$  rays emitted by particles moving at  $\beta = 0.6$ . A (relative) 5% discrepancy between the simulation and source calibration was observed and included in the systematic uncertainties of the cross sections.

Considering the neutron separation energy  $S_n = 3190(40)$  keV of  $^{53}\text{Ca}$  [11], final states may include unbound states, which are followed by neutron emission [41]. These beam-velocity neutrons were detected by two large-acceptance plastic scintillator arrays, NeuLAND demonstrator [42] and NEBULA [36,43], placed at zero degree, about 11 and 14 m downstream of the target, respectively. The NeuLAND array consisted of 400 modules ( $5 \times 5 \times 250$  cm<sup>3</sup> each) in 8 layers, while the NEBULA array consisted of 120 modules ( $12 \times 12 \times 180$  cm<sup>3</sup> each) and arranged in a two-wall configuration. The total  $1n$  detection efficiency of the combined array was obtained from simulation.

The Doppler-corrected  $\gamma$ -ray spectrum in coincidence with the  $^{54}\text{Ca}(p, pn)^{53}\text{Ca}$  channel is shown in Fig. 2(a). Add-back analysis was performed if at least two crystals within a 15 cm radius of each other's center detected a  $\gamma$  ray. The spectrum was fitted in the range of 1200–3000 keV with simulated DALI2<sup>+</sup> response functions added on an exponential background. Two peaks were fitted at 1738(17) and 2220(13) keV, respectively, while no coincidence was observed between them from the  $\gamma$ - $\gamma$  analysis [Fig. 2(c)]. These two peaks were consistent with the previously reported transitions from the  $\beta$ -decay study [31] and the in-beam  $\gamma$ -ray study [12], where they were placed in parallel from two excited states directly decaying to the ground state. No further transition was observed below  $S_n$ ; thus no more bound states are expected to be populated in addition to the two excited states and the ground state.

A significant ratio of the events for Fig. 2(a) was found to have a neutron detected by the NeuLAND + NEBULA array. The  $\gamma$ -ray spectrum from these events [Fig. 2(b)] exhibited a very different  $\gamma$ -ray transition ratio from the original spectrum. The two-body relative energy for  $^{53}\text{Ca} + n$ , reconstructed from the momentum vectors of the fragment and the neutron, is shown in Fig. 2(d). These events originate from the inelastic excitation process beyond the  $S_n = 3.84(7)$  MeV of  $^{54}\text{Ca}$  [11] followed by neutron emission,  $^{54}\text{Ca}(p, p')^{54}\text{Ca}^* \rightarrow ^{53}\text{Ca} + n$ , mixed in the neutron knock-out channel, and as such were subtracted in cross section and momentum distribution. Their discussion [44] is beyond the scope of this Letter.

Determined inclusive and exclusive cross sections for the  $^{54}\text{Ca}(p, pn)^{53}\text{Ca}$  reaction are summarized in Table I, for which the component to the ground state was extracted by subtracting the two excited states from the inclusive cross section. Furthermore, contributions from the  $^{54}\text{Ca}(p, p')^{54}\text{Ca}^* \rightarrow ^{53}\text{Ca} + n$  channel were subtracted using the fitted peak intensities corrected with the  $1n$ -detection

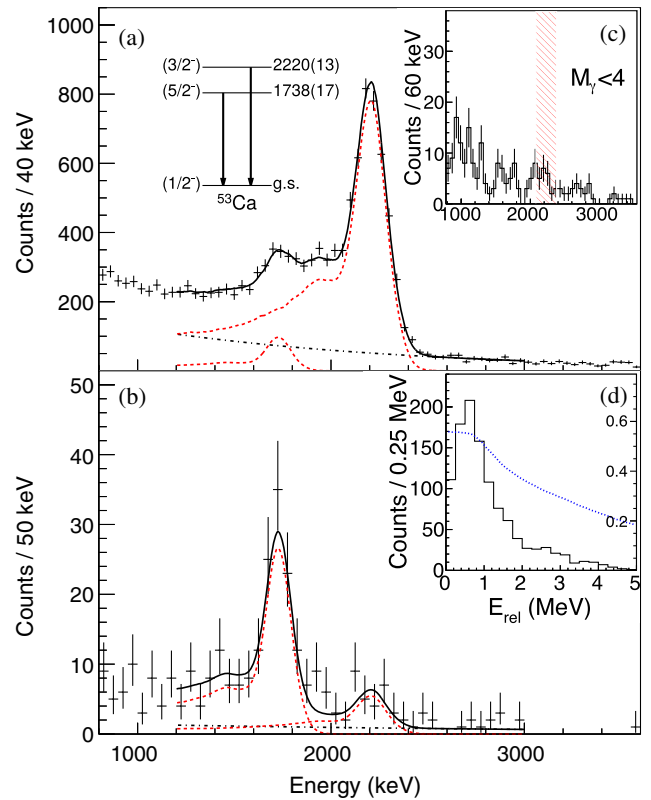


FIG. 2. (a) Doppler-corrected  $\gamma$ -ray spectrum in coincidence with the  $^{54}\text{Ca}(p, pn)^{53}\text{Ca}$  channel, fitted with simulated response functions (red) and exponential background (black). (b) Same Doppler-corrected  $\gamma$ -ray spectrum, but in coincidence with a detected neutron. (c) The  $\gamma$ -ray spectrum in coincidence with the 2220-keV transition. The red-hatched area represents the gate used in  $\gamma$ - $\gamma$  analysis. (d) Relative energy spectrum of  $^{53}\text{Ca} + n$  for which the dotted line represents the simulated neutron detection efficiency with the scale on the right side.

efficiency from simulation. This channel contributes 7(3)%, 1.1(3)%, and 44(11)% to the  $1/2^-$ ,  $3/2^-$ , and  $5/2^-$  states in the mixed data.

Evidently, the cross section of 19.1(12) mb for the 2220-keV final state is about 20 times larger than the one for the 1738-keV final state. In a simple picture with the  $f_{5/2}$  orbital well above the  $p_{3/2}$  and  $p_{1/2}$  orbitals, the ground state of  $^{54}\text{Ca}$  has completely filled neutron  $p_{3/2}$  and  $p_{1/2}$  orbitals, and an empty  $f_{5/2}$  orbital. This results in the dominance of  $3/2^-$  and  $1/2^-$  states in  $^{53}\text{Ca}$  populated following the  $^{54}\text{Ca}(p, pn)$  reaction. Obtained cross sections are consistent with this picture and the tentative spin-parity assignments, but can be substantiated further by orbital angular momentum ( $l$ -value) assignments from momentum extraction of the  $^{53}\text{Ca}$  residues in the center of mass frame of  $^{54}\text{Ca}$ .

The momentum distributions were extracted using the beam and fragment velocities at the reconstructed reaction vertex, as well as the scattering angle measured by drift chambers placed in front and behind the secondary target.



TABLE I. Inclusive and exclusive cross sections (in mbarn) for the  $^{54}\text{Ca}(p, pn)^{53}\text{Ca}$  reaction ( $\sigma_{-1n}$ ), compared with theoretical values ( $\sigma_{-1n}^{\text{th}}$ ) using the calculated single-particle cross sections ( $\sigma_{\text{sp}}$ ) from the DWIA framework and spectroscopic factors ( $C^2S$ ) from SM (GXPF1Bs). The  $\sigma_{-1n}^{\text{th}}$  of *ab initio* calculations [NNLOsat and NN+3N(Inl)] are obtained with microscopic OFs (instead of Ref. [45]) as described in the text. The assigned  $J^\pi$  and the corresponding neutron removal orbitals are also given.

|           | $J^\pi$ | $-1n$     | $\sigma_{-1n}$ | DWIA                 |             | GXPF1Bs |                            | NNLO <sub>sat</sub> |        |                            | NN + 3N (Inl) |        |                            |
|-----------|---------|-----------|----------------|----------------------|-------------|---------|----------------------------|---------------------|--------|----------------------------|---------------|--------|----------------------------|
|           |         |           |                | $\sigma_{\text{sp}}$ | $E_x$ (keV) | $C^2S$  | $\sigma_{-1n}^{\text{th}}$ | $E_x$ (keV)         | $C^2S$ | $\sigma_{-1n}^{\text{th}}$ | $E_x$ (keV)   | $C^2S$ | $\sigma_{-1n}^{\text{th}}$ |
| g.s.      | $1/2^-$ | $p_{1/2}$ | 15.9(17)       | 7.27                 | 0           | 1.82    | 13.2                       | 0                   | 1.56   | 11.3                       | 0             | 1.58   | 11.6                       |
| 2220(13)  | $3/2^-$ | $p_{3/2}$ | 19.1(12)       | 6.24                 | 2061        | 3.55    | 22.2                       | 2635                | 3.12   | 18.5                       | 2611          | 3.17   | 17.0                       |
| 1738(17)  | $5/2^-$ | $f_{5/2}$ | 1.0(3)         | 4.19                 | 1934        | 0.19    | 0.8                        | 1950                | 0.01   | 0.1                        | 2590          | 0.02   | 0.1                        |
| Inclusive |         |           | 36.0(12)       |                      |             |         | 36.2                       |                     |        | 29.9                       |               |        | 28.7                       |

For parallel momentum, a resolution of 40 MeV/c (sigma) was obtained from the unreacted  $^{54}\text{Ca}$  beam. The uncertainty of the reaction vertex position was also considered and taken into account when convoluting the resolution to theoretical predicted momentum distributions. The momentum distributions for the two excited states were extracted by fitting the  $\gamma$ -ray spectra in coincidence with the selection of 40 MeV/c -width sections of the inclusive momentum distribution.

Figure 3(a) illustrates the inclusive parallel momentum distributions for the  $(p, pn)$  and  $pp' \rightarrow n$  channels. The distribution of  $(p, pn)$  was centered close to zero, while the one of  $pp' \rightarrow n$  was clearly shifted, thus providing an additional evidence for the existence of the  $pp' \rightarrow n$  channel in the data. Figures 3(b)–3(d) show the parallel momentum distributions associated with the final states of the  $^{54}\text{Ca}(p, pn)^{53}\text{Ca}$  reaction. Similar to the exclusive cross

sections, the distribution for the ground state was extracted by subtracting the excited state distributions from the inclusive one. Results of the transverse momentum distribution analysis are illustrated in Fig. 4 with the same panel arrangement as Fig. 3.

Experimental results were confronted with calculated single-particle cross sections ( $\sigma_{\text{sp}}$ ) and momentum distributions of neutron removal from  $p_{1/2}$ ,  $p_{3/2}$ ,  $f_{5/2}$  orbitals populating each final state in  $^{53}\text{Ca}$  using the distorted wave impulse approximation (DWIA) model [46,47]. In this DWIA approach, already applied in earlier works [48–50], the single-particle wave function and the nuclear density of  $^{54}\text{Ca}$  were calculated using the single-particle potential by Ref. [45], with the depth tuned to reproduce the experimental energies. Optical potentials for the distorted waves in the initial and final states were constructed by the microscopic folding model [51], employing the Melbourne  $g$  matrix  $NN$  interaction [52] and the calculated nuclear density. Finally, the Franey-Love effective interaction [53] was implemented for the  $pn$  interaction. The ground state [Figs. 3 and 4(b)] and the 2220-keV distribution [Figs. 3 and 4(c)] were well reproduced by the

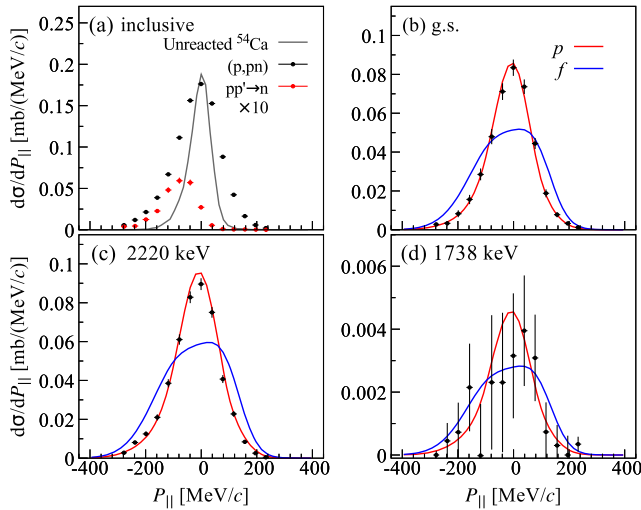


FIG. 3. (a) Inclusive parallel momentum distributions of the  $^{53}\text{Ca}$  residues for  $^{54}\text{Ca}(p, pn)^{53}\text{Ca}$  channel (black) and  $^{54}\text{Ca}(p, p')^{54}\text{Ca}^* \rightarrow ^{53}\text{Ca} + n$  channel (red, amplitude  $\times 10$  for display). The dot-dashed line shows the intrinsic resolution of the setup. Exclusive momentum distributions for (b) g.s., (c) 2220-keV, and (d) 1738-keV states, compared with calculated DWIA distributions assuming  $1n$  removal from  $p$  and  $f$  orbitals. Error bars are dominated by statistical errors. See text for details.

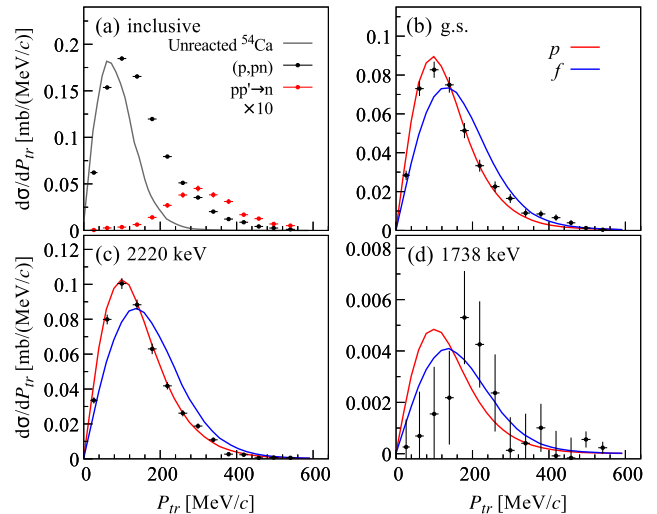


FIG. 4. The same as Fig. 3 for transverse momentum distributions.

DWIA calculated  $p$  curve, providing evidence for the  $l = 1$  assignments of these states. However, the low intensity and low peak-to-background ratio of the 1738-keV transition resulted in large error bars, not permitting distinction between  $p$  or  $f$  curves for parallel momentum, while for transverse momentum, the experimental data fitted better with an  $f$  wave.

The single-particle cross sections  $\sigma_{\text{sp}}$ , calculated in the DWIA and averaged along the thick target, are shown in Table I, and allow us to extract the spectroscopic factors  $C^2S$  as ratios with the measured cross sections. A systematic uncertainty of 15% was considered for the calculated  $\sigma_{\text{sp}}$  [47]. The DWIA  $\sigma_{\text{sp}}$  are consistent with the results from the transfer to the continuum model [54,55]. This leads to spectroscopic factors of 2.2(2)(3), 3.1(2)(5), and 0.23(7)(3) for the first  $1/2^-$ ,  $3/2^-$ , and  $5/2^-$  states, respectively. The first error indicates the statistical error from the data, while the second error originates from the uncertainty of  $\sigma_{\text{sp}}$ . Large  $p$  strength and little  $f$  strength are observed in low excitation states of  $^{53}\text{Ca}$  from the one-neutron removal from  $^{54}\text{Ca}$ , providing strong evidence to the nature of  $N = 34$  shell closure.

The present salient closed-shell feature can be studied in more detail by confronting it with theoretical inclusive and exclusive cross sections. They are obtained by combining the  $\sigma_{\text{sp}}$  values discussed above with  $C^2S$  values from the shell model or by the *ab initio* calculations described below.

For shell-model studies of Ca isotopes, the GXPF1 family of effective interactions [25] has often been used. For example, the measurement of  $E(2_1^+)$  in Ref. [12] was compared to calculations with the GXPF1Br interaction [56]. Here we introduce the GXPF1Bs interaction, where the  $\nu f_{5/2}^2$  pairing matrix element is shifted by  $-0.4$  MeV from the GXPF1Br value so that the  $\nu f_{7/2}^2$  and  $\nu f_{5/2}^2$  pairing matrix elements can be better factorized by the orbital occupation number,  $(2j + 1)$ . We therefore use the GXPF1Bs interaction, although there are no notable differences from GXPF1Br results. The calculation results are shown in Table I. The remarkable agreement between the calculated cross sections and the experimental values supports the tensor-force-driven  $N = 34$  magicity.

It is interesting to note that as the  $E(2_1^+)$  of  $^{54}\text{Ca}$  is 0.5 MeV lower than that of  $^{52}\text{Ca}$ , one may expect that the closed shell structure is weaker in  $^{54}\text{Ca}$  than in  $^{52}\text{Ca}$ . The shell-model calculated spectroscopic factor for the  $\nu p_{1/2}$  orbital in  $^{54}\text{Ca}$  ground state is 91% of the maximum value, being larger than the corresponding 89% for the  $\nu p_{3/2}$  orbital in the  $^{52}\text{Ca}$  ground state. This suggests a more robust subshell closure of  $N = 34$  than  $N = 32$ . We can compare the present 91% to the experimental one of  $^{48}\text{Ca}$  reported as 92% [57]. Thus, the subshell closure at  $N = 34$  for  $^{54}\text{Ca}$  is identified to be comparable with the well-established one at  $N = 28$  for  $^{48}\text{Ca}$ . We stress that although the  $E(2_1^+)$  value provides a global landscape, it can be misleading due to a “local” refined behavior. In the present case, this is

explained by the repulsive contribution from the tensor force to the  $\nu p_{1/2}^2$  pairing matrix element, which lowers the  $E(2_1^+)$  without disturbing the closed shell formation. This notion reinforces the necessity of reaction experiments like this work, and a similar experiment on  $^{52}\text{Ca}$  is of interest.

Theoretical cross sections were also computed using microscopic  $C^2S$  and overlap functions (OFs) obtained from *ab initio* self-consistent Green’s function (SCGF) theory [58]. SCGF calculations were carried out in a model space containing up to 14 harmonic oscillator shells and employed the third-order algebraic diagrammatic construction scheme [59], which has been shown to provide precise results in light and medium-mass nuclei [60,61]. Two different  $NN + 3N$  chiral interactions were employed: the NNLO<sub>sat</sub> introduced in Ref. [62] has provided accurate predictions of nuclear radii in several recent state-of-the-art *ab initio* calculations [61,63,64]. The second Hamiltonian is the newly developed  $NN + 3N(\text{nl})$  with both local and nonlocal  $3N$  regulators. It has yielded promising results for isotopes near neutron-rich titanium [21,65].

In SCGF theory, one-nucleon removal energies and  $C^2S$  as well as associated OFs are directly obtained from the spectral representation of the single-particle GF [58].  $C^2S$  and OFs are then inserted in the DWIA calculation together with the optical potential and  $pn$  interaction. The optical potential is generated by the folding model [51] with the Melbourne  $g$ -matrix interaction [52] and the nuclear density obtained by SCGF. Although this does not yet lead to complete *ab initio* cross sections, it allows us to test consistent *ab initio* ingredients in the reaction model. A similar method was used in Ref. [66], where the resulting rms radii of the OFs were compared with the experimental ones and readjusted to overcome the problems related to the known underestimation of radii with the standard chiral interactions. Since the present interactions yield a much improved description of these observables, no rescaling was employed here.

Altogether, *ab initio* and shell-model results give a remarkably consistent interpretation of the measured cross sections and the resulting energies and  $C^2S$  strongly reinforce the experimental spin assignments. Nevertheless, there are some discrepancies. The SCGF computes the eigenstates of  $^{53}\text{Ca}$  either as neutron removal (addition) energies from  $^{54}\text{Ca}$  (to  $^{52}\text{Ca}$ ). Table I shows energies,  $C^2S$  and  $\sigma_{-1n}^{\text{th}}$  for the  $^{54}\text{Ca}-1n$  case that is relevant to the present study. The *ab initio*  $C^2S$  are consistently lower than the GXPF1 ones due to coupling to collective excitations that are excluded from SM valence spaces [67]. Thus, correlation effects for the dominant  $1/2^-$  and  $3/2^-$  hole states appear to be stronger in SCGF. Conversely, the  $5/2^-$  state is not a dominant hole state and requires configuration mixing contributions that are better accounted for by the SM. Both chiral interactions overestimate the  $1/2^-$ - $3/2^-$  energy splitting at around 2.6 MeV. If, instead, we perform SCGF calculations for neutron addition to  $^{52}\text{Ca}$ , both the

ground and  $5/2^-$  states of  $^{53}\text{Ca}$  are dominant quasiparticle orbits and their energy difference is evaluated accurately. In this case,  $\text{NNLO}_{\text{sat}}$  and  $NN + 3N(\text{ln}l)$  predict 1.40 and 1.99 MeV, respectively, with the latter being now closer to experiment.

In summary, inclusive and exclusive cross sections from the  $^{54}\text{Ca}(p, pn)^{53}\text{Ca}$  reaction at 216 MeV/ $u$  were measured based on the in-beam  $\gamma$  technique at RIBF. For the first time, both the exclusive parallel and transverse momentum distributions for quasifree knock-out reaction from a proton target were measured, providing experimental evidence for the orbital angular momentum assignments in  $^{53}\text{Ca}$ . The measured cross section to the  $p_{3/2}$  state of  $^{53}\text{Ca}$  is about 20 times larger than the one to the  $f_{5/2}$  state. Such little  $f$  wave component in the ground state of  $^{54}\text{Ca}$  provides direct evidence of the  $N = 34$  subshell closure. The experimental data were reproduced by the DWIA reaction model together with structure input from the shell-model calculation using GXPFBs interaction and *ab initio* calculations with  $\text{NNLO}_{\text{sat}}$  and  $NN + 3N(\text{ln}l)$  interactions. By comparing with the calculated  $\sigma_{\text{sp}}$ , the experimental spectroscopic factors were obtained to be 2.2(2)(3), 3.1(2)(5), and 0.23(7)(3) for the  $1/2^-$ ,  $3/2^-$ , and  $5/2^-$  states, concluding a good  $N = 34$  magicity.

We would like to express our gratitude to the RIKEN Nishina Center accelerator staff for providing the stable and high-intensity beam and to the BigRIPS team for operating the secondary beams. We are thankful to Dr. M. Gomez-Ramos for discussion on reaction models. S. C. acknowledges the support of the IPA program at RIKEN Nishina Center. J. L. acknowledges the support from Research Grants Council (RGC) of Hong Kong with grant of Early Career Scheme (ECS-27303915). K. O., K. Y., and Y. C. acknowledge the support from Grants-in-Aid of the Japan Society for the Promotion of Science under Grants No. JP16K05352. Y. L. S. acknowledges the support of the Marie Skłodowska-Curie Individual Fellowship (H2020-MSCA-IF-2015-705023). V. V. acknowledges support from the Spanish Ministerio de Economía y Competitividad under Contract No. FPA2017-84756-C4-2-P. L. X. C. and B. D. L. would like to thank MOST for its support through the Physics Development Program Grant No. ĐTĐLCN.25/18. D. R. and V. W. acknowledge the Deutsche Forschungsgemeinschaft (DFG, German Research Foundation) under Grant No. SFB1245. V. W. and P. K. acknowledge the German BMBF Grant No. 05P19RDFN1. P. K. was also supported by HGS-HIRE. D. S. was supported by Projects No. GINOP-2.3.3-15-2016-00034 and No. NKFIH-NN114454. I. G. has been supported by HIC for FAIR and Croatian Science Foundation under Projects No. 1257 and No. 7194. K. I. H., D. K., and S. Y. P. acknowledge the support from the NRF grant funded by the Korea government (No. 2016K1A3A7A09005580 and No. 2018R1A5A1025563). This work was also supported by the United Kingdom Science and Technology Facilities Council (STFC) under Grants No. ST/P005314/1 and

No. ST/L005816/1, and by NKFIH (128072), and by JSPS KAKENHI Grant No. 16H02179, and by MEXT KAKENHI Grant No. 18H05404. The development of MINOS were supported by the European Research Council through the ERC Grant No. MINOS-258567. Green's function calculations were performed using HPC resources from the DiRAC Data Intensive service at Leicester, UK (funded by the UK BEIS via STFC capital Grants No. ST/K000373/1 and No. ST/R002363/1 and STFC DiRAC Operations Grant No. ST/R001014/1) and from GENCI-TGCC, France (Project No. A0050507392).

\*sdchen@hku.hk

†jleehc@hku.hk

- [1] O. Haxel, J. Hans, D. Jensen, and H. E. Suess, *Phys. Rev.* **75**, 1766 (1949).
- [2] M. G. Mayer, *Phys. Rev.* **75**, 1969 (1949).
- [3] C. Détraz, D. Guillemaud, G. Huber, R. Klapisch, M. Langevin, F. Naulin, C. Thibault, L. C. Carraz, and F. Touchard, *Phys. Rev. C* **19**, 164 (1979).
- [4] D. Guillemaud-Mueller, C. Detraz, M. Langevin, F. Naulin, M. de Saint-Simon, C. Thibault, F. Touchard, and M. Epherre, *Nucl. Phys.* **A426**, 37 (1984).
- [5] T. Motobayashi *et al.*, *Phys. Lett. B* **346**, 9 (1995).
- [6] B. Bastin *et al.*, *Phys. Rev. Lett.* **99**, 022503 (2007).
- [7] S. Takeuchi *et al.*, *Phys. Rev. Lett.* **109**, 182501 (2012).
- [8] C. R. Hoffman *et al.*, *Phys. Rev. Lett.* **100**, 152502 (2008).
- [9] C. Hoffman *et al.*, *Phys. Lett. B* **672**, 17 (2009).
- [10] R. Kanungo *et al.*, *Phys. Rev. Lett.* **102**, 152501 (2009).
- [11] F. Wienholtz *et al.*, *Nature (London)* **498**, 346 (2013).
- [12] D. Steppenbeck *et al.*, *Nature (London)* **502**, 207 (2013).
- [13] O. Sorlin and M.-G. Porquet, *Prog. Part. Nucl. Phys.* **61**, 602 (2008).
- [14] T. Otsuka, *Phys. Scr.* **2013**, 014007 (2013).
- [15] D. Steppenbeck *et al.*, *Phys. Rev. Lett.* **114**, 252501 (2015).
- [16] A. Huck, G. Klotz, A. Knipper, C. Miehé, C. Richard-Serre, G. Walter, A. Poves, H. L. Ravn, and G. Marguier, *Phys. Rev. C* **31**, 2226 (1985).
- [17] A. Gade *et al.*, *Phys. Rev. C* **74**, 021302 (2006).
- [18] X. L. Tu, X. G. Zhou, D. J. Vieira, J. M. Wouters, Z. Y. Zhou, H. L. Seifert, and V. G. Lind, *Z. Phys. A* **337**, 361 (1990).
- [19] R. Janssens *et al.*, *Phys. Lett. B* **546**, 55 (2002).
- [20] D.-C. Dinca *et al.*, *Phys. Rev. C* **71**, 041302 (2005).
- [21] E. Leistenschneider *et al.*, *Phys. Rev. Lett.* **120**, 062503 (2018).
- [22] J. Prisciandaro *et al.*, *Phys. Lett. B* **510**, 17 (2001).
- [23] A. Bürger *et al.*, *Phys. Lett. B* **622**, 29 (2005).
- [24] T. Otsuka, R. Fujimoto, Y. Utsuno, B. A. Brown, M. Honma, and T. Mizusaki, *Phys. Rev. Lett.* **87**, 082502 (2001).
- [25] M. Honma, T. Otsuka, B. A. Brown, and T. Mizusaki, *Eur. Phys. J. A* **25**, 499 (2005).
- [26] T. Otsuka, T. Suzuki, R. Fujimoto, H. Grawe, and Y. Akaishi, *Phys. Rev. Lett.* **95**, 232502 (2005).
- [27] T. Otsuka and Y. Tsunoda, *J. Phys. G* **43**, 024009 (2016).
- [28] S. N. Liddick *et al.*, *Phys. Rev. Lett.* **92**, 072502 (2004).

- [29] S. Michimasa *et al.*, *Phys. Rev. Lett.* **121**, 022506 (2018).
- [30] H. N. Liu *et al.*, *Phys. Rev. Lett.* **122**, 072502 (2019).
- [31] F. Perrot *et al.*, *Phys. Rev. C* **74**, 014313 (2006).
- [32] T. Kubo *et al.*, *Prog. Theor. Exp. Phys.* **2012**, 03C003 (2012).
- [33] T. Kubo, *Nucl. Instrum. Methods Phys. Res., Sect. B* **204**, 97 (2003).
- [34] N. Fukuda, T. Kubo, T. Ohnishi, N. Inabe, H. Takeda, D. Kameda, and H. Suzuki, *Nucl. Instrum. Methods Phys. Res., Sect. B* **317**, 323 (2013).
- [35] A. Obertelli *et al.*, *Eur. Phys. J. A* **50**, 8 (2014).
- [36] T. Kobayashi *et al.*, *Nucl. Instrum. Methods Phys. Res., Sect. A* **317**, 294 (2013).
- [37] C. Santamaria *et al.*, *Nucl. Instrum. Methods Phys. Res., Sect. A* **905**, 138 (2018).
- [38] S. Takeuchi, T. Motobayashi, Y. Togano, M. Matsushita, N. Aoi, K. Demichi, H. Hasegawa, and H. Murakami, *Nucl. Instrum. Methods Phys. Res., Sect. A* **763**, 596 (2014).
- [39] I. Murray *et al.*, *RIKEN Accel. Prog. Rep.* **51**, 158 (2018).
- [40] S. Agostinelli *et al.*, *Nucl. Instrum. Methods Phys. Res., Sect. A* **506**, 250 (2003).
- [41] J. Lee *et al.* (to be published).
- [42] T. Aumann, Technical Report for the design, construction and commissioning of NeuLAND: The high-resolution neutron time-of-flight spectrometer for R3B, Technical Report, FAIR, 2011.
- [43] T. Nakamura and Y. Kondo, *Nucl. Instrum. Methods Phys. Res., Sect. B* **376**, 156 (2016).
- [44] F. Browne *et al.* (to be published).
- [45] A. Bohr and B. Mottelson, *Nuclear Structure* (World Scientific, Singapore, 1999), Vol. I.
- [46] K. Ogata, K. Yoshida, and K. Minomo, *Phys. Rev. C* **92**, 034616 (2015).
- [47] T. Wakasa, K. Ogata, and T. Noro, *Prog. Part. Nucl. Phys.* **96**, 32 (2017).
- [48] L. Olivier *et al.*, *Phys. Rev. Lett.* **119**, 192501 (2017).
- [49] Z. Elekes *et al.*, *Phys. Rev. C* **99**, 014312 (2019).
- [50] R. Taniuchi *et al.*, *Nature (London)* **569**, 53 (2019).
- [51] M. Toyokawa, K. Minomo, and M. Yahiro, *Phys. Rev. C* **88**, 054602 (2013).
- [52] K. Amos, P. Dortmans, H. von Geramb, S. Karataglidis, and J. Raynal, *Adv. Nucl. Phys.* **25**, 275 (2000).
- [53] M. A. Franey and W. G. Love, *Phys. Rev. C* **31**, 488 (1985).
- [54] M. Gomez-Ramos (private communication).
- [55] A. M. Moro, *Phys. Rev. C* **92**, 044605 (2015).
- [56] Y. Utsuno, T. Otsuka, Y. Tsunoda, N. Shimizu, M. Honma, T. Togashi, and T. Mizusaki, *JPS Conf. Proc.* **6**, 010007 (2015).
- [57] J. Lee, M. B. Tsang, and W. G. Lynch, *Phys. Rev. C* **75**, 064320 (2007).
- [58] C. Barbieri and A. Carbone, *Lect. Notes Phys.* **936**, 571 (2017).
- [59] F. Raimondi and C. Barbieri, *Phys. Rev. C* **97**, 054308 (2018).
- [60] A. Cipollone, C. Barbieri, and P. Navrátil, *Phys. Rev. C* **92**, 014306 (2015).
- [61] T. Duguet, V. Somà, S. Lecluse, C. Barbieri, and P. Navrátil, *Phys. Rev. C* **95**, 034319 (2017).
- [62] A. Ekström, G. R. Jansen, K. A. Wendt, G. Hagen, T. Papenbrock, B. D. Carlsson, C. Forssén, M. Hjorth-Jensen, P. Navrátil, and W. Nazarewicz, *Phys. Rev. C* **91**, 051301(R) (2015).
- [63] R. Garcia Ruiz *et al.*, *Nat. Phys.* **12**, 594 (2016).
- [64] V. Lapoux, V. Somà, C. Barbieri, H. Hergert, J. D. Holt, and S. R. Stroberg, *Phys. Rev. Lett.* **117**, 052501 (2016).
- [65] V. Somà, F. Raimondi *et al.* (to be published).
- [66] F. Flavigny *et al.*, *Phys. Rev. Lett.* **110**, 122503 (2013).
- [67] C. Barbieri, *Phys. Rev. Lett.* **103**, 202502 (2009).